Three-dimensional vortex structures in a cylinder wake

By J. WU[1], J. SHERIDAN[2], M. C. WELSH[1] AND K. HOURIGAN[2]

[1] CSIRO Division of Building, Construction and Engineering, Highett, Victoria 3190, Australia

[2] Department of Mechanical Engineering, Monash University, Clayton, Victoria 3168, Australia

The three-dimensionality of the velocity field in the wake of a circular cylinder has excited considerable interest and debate over the past decade. Presented here are experimental results that characterize the underlying vorticity field of such wakes. Using particle image velocimetry (PIV), instantaneous velocity fields were measured and from these the vorticity of the longitudinal vortices lying in the region between Kármán vortices was found. Near the saddle point, induced by the stretching of the Kármán vortices, the vorticity of the longitudinal vortices was found to be greater than the Kármán vortices themselves. Their circulation was of the order of 10% of the Kármán vortices. The high levels of vorticity result from the stretching of the longitudinal vortices, as evident in the topology of the vortices. It is shown that the longitudinal vortices are locked in phase to the Kármán vortices, effectively riding on their backs in the braid region. While only one mode of longitudinal vortex formation was observed, evidence was found of a step change in the vorticity levels at a Reynolds number of approximately 200. This is consistent with the transition point between the two modes of vortex shedding shown to exist by Williamson (1988). It had previously been proposed that the observed vortex patterns were consistent with the evolution of the longitudinal vortices from perturbations of vortex lines in the separating shear layer which experience self-induction and stretching from the Kármán vortices. Evidence is presented that supports this model.

1. Introduction

The wake of a circular cylinder has a special place in the study of bluff-body wakes. Historically, the problem has attracted leaders in the field, as evident by the terms 'Strouhal shedding' and 'Kármán vortices'. However, it has also been of great interest to engineers because it either appears in so many technological devices, such as cross-flow heat exchangers and offshore or onshore structures, or serves as a simplified, but useful, model for the more complicated geometries of practical interest. Over the past decade, however, several new stimuli have caused a re-examination of the problem at a fundamental level.

Roshko (1955), in his early and comprehensive review of cylinder wakes, noted an inconsistency in the relationship between the Strouhal and Reynolds numbers at Reynolds numbers between 150 and 300. He interpreted this as a transition range and noted that velocity measurements were erratic in this range. Roshko's primary focus was on turbulence with the cylinder wake being used as a test case for turbulence in

wakes and behind grids, an instance of the use of cylinder wakes as a canonical flow problem for the study of a wider problem. Hama (1957), in an early study, recognized that the wake of cylinders was three-dimensional when he found that a transverse waviness appeared in his flow visualization at Reynolds numbers greater than 150. Grant (1958), using hot-wire anemometry and cross-correlation techniques, studied the wake of circular cylinders in cross-flow. He found that above certain Reynolds numbers the Kármán vortices develop three-dimensionalities composed of counter-rotating streamwise vortices. Later, Gerrard (1978) conducted a flow visualization study of cylinder wakes in which he observed what he termed 'fingers' of dye forming along the span of his cylinder at Reynolds numbers above 140. With hindsight, it seems reasonable to conclude that the transverse waviness of Hama (1957) and the fingers of Gerrard (1978) resulted from the same phenomenon, i.e. the presence of vortices (known hereafter as longitudinal vortices) inclined at an angle to the streamwise direction.

Wei & Smith (1986), Williamson (1988), Welsh *et al.* (1992), Bays-Muchmore & Ahmed (1993) and Wu *et al.* (1994*a*, *d*) have in recent years presented direct evidence of the existence of the three-dimensional longitudinal vortices using flow visualization. Wu *et al.* (1994*d*) have presented preliminary results, based on particle image velocimetry (PIV), of the vorticity fields of the vortices, while Mansy, Yang & Williams (1994) have measured the velocity field using scanning laser anemometry. Both Mansy *et al.* (1994) and Wu *et al.* (1994*a*) have presented results of the measurement of the spanwise wavelength of the vortices and discussed its variation with Reynolds number.

The longitudinal vortices have also been found to exist at much higher Reynolds numbers in the last few years. Lin, Vorobieff & Rockwell (1995) used a cinematographic PIV technique to build three-dimensional structures in the near-wake region and showed the existence of longitudinal vortex structures at $Re = 10\,000$. Similar three-dimensional structures can be seen in the results of the large-eddy simulation of Gonze (1993), at a high Reynolds number.

In flow visualizations the longitudinal vortices appear as mushroom-type structures in the near wake. An examples is shown in figure 1. These are consistent with longitudinal vortices inclined to and superimposed on the Kármán vortices. Bernal & Roshko (1986) have shown that similar vortex structures appear to be superimposed on the large-scale vortices found in plane mixing layers.

Another case of the cylinder being considered as a test problem is in the matching of experiments and numerical studies. With advances in both computer hardware and numerical algorithms, it is now possible to resolve all scales of motion in modelling cylinder wakes at Reynolds numbers below 250. Given that the three-dimensionality is now established, the possibility exists to compare calculated and measured velocity and vorticity fields with the consequent enrichment to both sets of investigations. Karniadakis & Triantafyllou (1992) used a high-order time-accurate spectral element method to compute the flow in the wake of a circular cylinder at low Reynolds numbers. They found that the wake is inherently three-dimensional for Reynolds numbers greater than 200. At a Reynolds number of 225 a coherent three-dimensional 'rib-like' pattern evolved from a random initial disturbance.

Thompson, Hourigan & Sheridan (1994), in a study using a different spectral element method and a larger domain, observed both modes 'A' and 'B' of vortex shedding, as found experimentally by Williamson. The two modes have spanwise wavelengths of approximately 3 diameters and 0.8 diameters, respectively. Meiburg & Lasheras (1988) studied the three-dimensional wake which develops behind a flat plate having spanwise perturbations in its trailing edge. This was done using a vortex
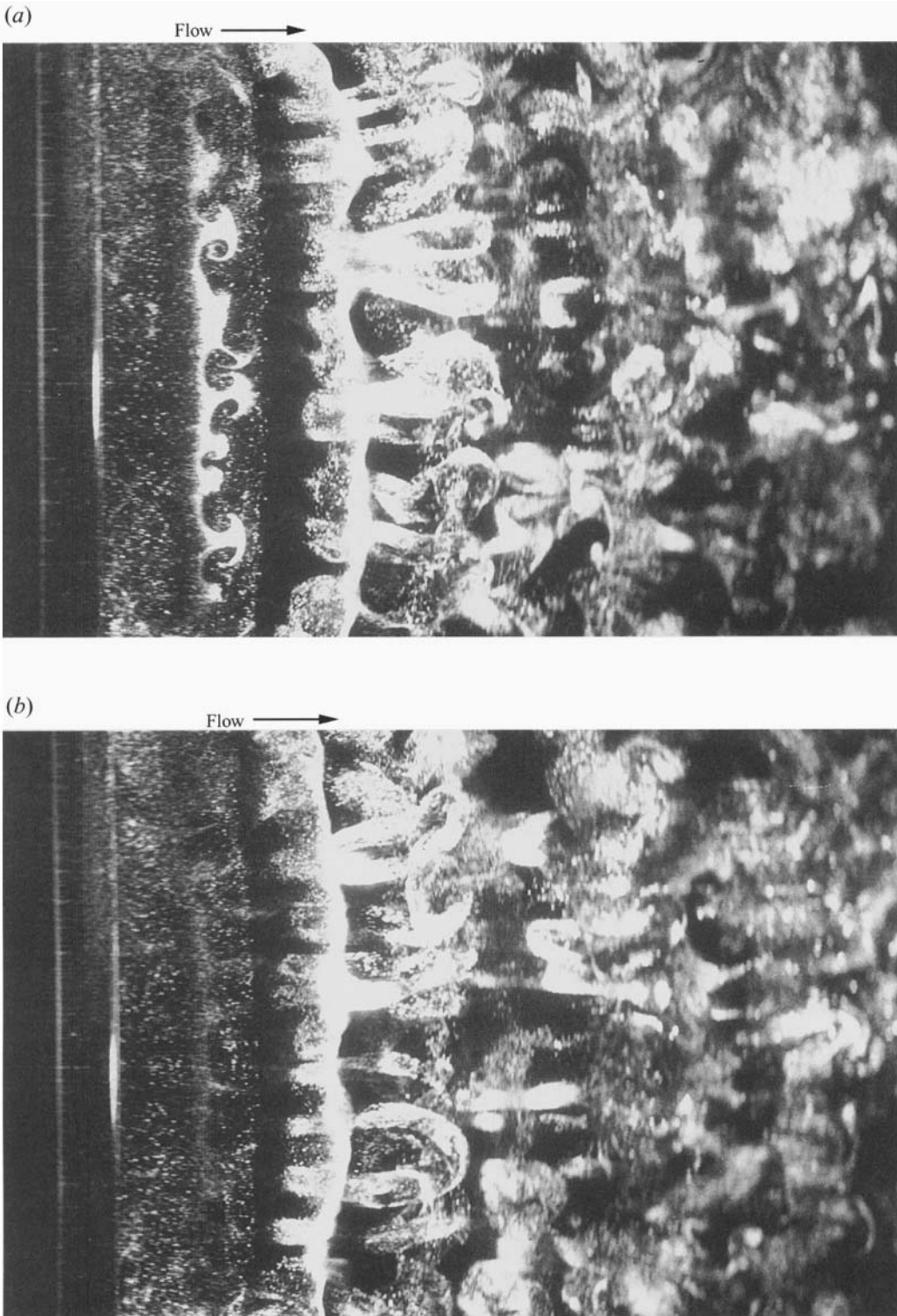
FIGURE 1. Counter-rotating longitudinal vortices in the centreline plane of a circular cylinder, $Re = 550$. Flow was visualized using hydrogen bubbles generated by a wire placed behind the cylinder. The flow is shown at two instants, (a) and (b), at different phases of Kármán vortex shedding cycle.

dynamics model for a Reynolds number of 100. They simulated the development of vortex filaments perturbed by the trailing edge well into the nonlinear regime and found that the most stretched filaments were those passing through the free-stagnation points. The redistribution, reorientation and stretching of vorticity leads to the formation of counter-rotating pairs of streamwise vortices superimposed on the large-scale wake vortices. Following this model, Wu, Sheridan & Welsh (1994c) developed an inviscid vortex dynamics model for the wake of a circular cylinder. They showed that any perturbation in a vortex line (or tube) in the separating shear layer can magnify, under the action of self-induction and stretching induced by the Kármán vortices, into rib-like vortices in the braid joining consecutive Kármán vortices. This is consistent with the model first proposed by Wei & Smith (1986) who suggested that the longitudinal vortices might result from vorticity present in the shear layer, the primary focus of their study.

Measurement of the velocity field in the wake of cylinders is essential for the better understanding of the structures and dynamics of three-dimensional wake flows. Owing to technical difficulties few attempts have been made to obtain such data. Hayakawa & Hussain (1989) used an X-wire rake to measure the transverse vorticity of the longitudinal vortices found in the intermediate region (10–20 diameters) of a cylinder wake. Their data, taken at a higher Reynolds number than examined in the present study, show the footprint of longitudinal vortices in the wake; they suggest that the three-dimensional character of the wake could be described as ribs wrapping around rolls or ribs in the braid.

In the study described here, digital particle image velocimetry (PIV) was used to measure the instantaneous velocity field in a transverse plane in the near wake of the cylinder. This plane contains the information needed to characterize the vorticity field associated with the longitudinal vortices. PIV, because it captures the full velocity field at one instant, is particularly well-suited to capturing such vortex structures. From the measured velocity fields the vorticity, circulation, geometry and topology of the longitudinal vortices has been extracted and is presented below.

2. Experimental apparatus and method

2.1. *Apparatus*

All experiments were conducted in the return-circuit water tunnel at CSIRO, Highett, Australia, as shown in figure 2. Water was pumped through a straight measurement section containing a calibrated orifice plate, through a diffuser and into a settling chamber containing filter material and a honeycomb. The water then passed through a 4:1 two-dimensional contraction and a 660 mm long straight square section before entering the working section. The working section was 770 mm long and 244 × 244 mm cross-section, and had transparent walls made of acrylic. Water left the working section via a 440 mm long duct from which it passed into an outlet reservoir tank. The free-stream velocity in the working section was uniform to within 1% outside the boundary layers at the walls. The spectrum of the fluctuating longitudinal velocity was free of sharp peaks and decreased in amplitude by 20 dB/Hz above 0.08 Hz; the longitudinal turbulence was, typically, 0.15%.

Circular cylinders made of Plexiglas, 244 mm long and with diameters of 6.4 and 9.4 mm, were used for the wake measurements. Ideally, one would prefer to conduct the experiment with an infinitely long cylinder in order to examine the flow-intrinsic three-dimensionalities of the vortex street behind a cylinder in a perfect two-dimensional
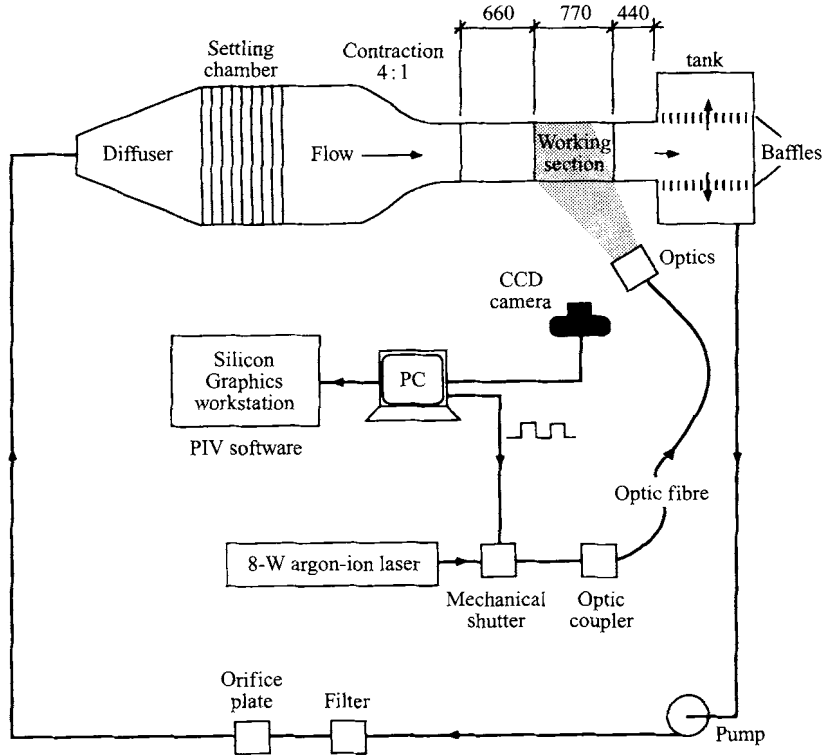
FIGURE 2. Schematic of experimental apparatus showing the return-circuit water tunnel, laser and CCD camera system used in producing images for PIV.

cross-flow. In practice this is not possible and the end effects of a finite length cylinder produce oblique vortex shedding at low Reynolds numbers. Williamson (1989) demonstrated that the end effects can be minimized by arranging the end plates at an inclined angle, inducing a parallel vortex shedding mode. His method was used here with a pair of end plates placed at an angle of 25° to the streamwise coordinate to ensure parallel vortex shedding when using flow visualization, thus minimizing end effects.

2.2. Method

All data presented were obtained using the digital PIV method. The review of Adrian (1991) provides an excellent overview of PIV; the detail of the method used here is available in the paper by Wu *et al.* (1994*b*). A brief description follows. Flow was seeded with white 'hollow' microspheres with a mean diameter < 30 μm. Light from an 6 W argon-ion continuous-beam laser was transmitted through a 50 μm diameter multi-mode optical fibre and spread into a light sheet using a cylindrical lens. The laser light was pulsed using a mechanical shutter installed in front of the fibre-optics input coupler. Light scattered from the particles in the laser sheet was recorded using a 'Videk' digital CCD camera, with a spatial resolution of 1280 × 1024 pixels; and the light intensity signal was digitized into 256 levels (8-bit) on a 386 personal computer. The velocity field was extracted from the particle image on a Silicon Graphics workstation using an in-house digital PIV software system based on a digital Young's fringe method.

The primary independent variable used in the study was the Reynolds number based
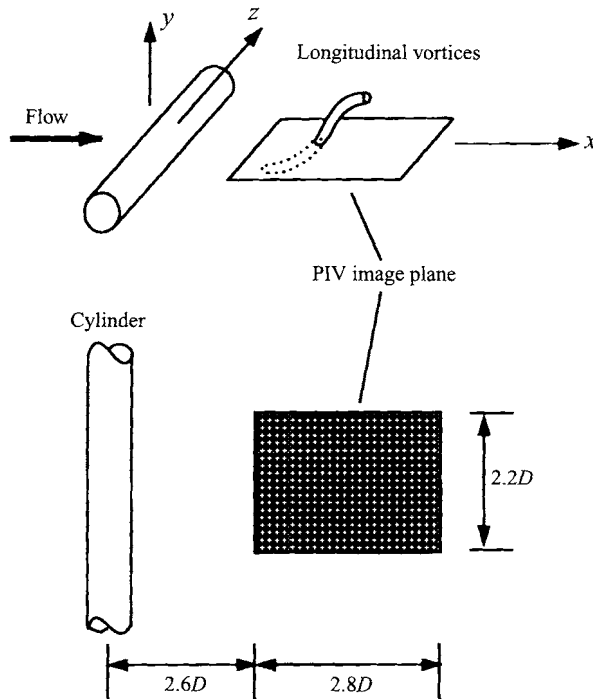
FIGURE 3. Schematic showing the coordinate system and PIV image plane used in measuring the flow field containing longitudinal vortices.

on cylinder diameter and free-stream velocity. Data were collected for a Reynolds number range of 140–550 but most of the data presented were recorded at a Reynolds number of 525. This value was chosen because it is well beyond the transition region for the onset of longitudinal vortex structures (Williamson 1988; Wu *et al.* 1994*a*), thus the longitudinal vortex structures should be fully developed and representative of a wider range of Reynolds numbers. The primary primitive dependent variables were the two components of the velocity field in the plane of the laser sheet, from which the vorticity in the orthogonal direction could be derived.

Also extracted from the velocity field were the 'sectional streamline patterns', as termed by Perry & Steiner (1987). They are representative of the instantaneous flow in a plane cutting through the three-dimensional flow field. These streamlines can be used to examine the flow topology in terms of critical points as first classified by Perry & Fairlie (1974). Streamlines were obtained by integrating the velocity field with a predictor-corrector scheme from a prescribed starting value. Bi-linear interpolation of the measured velocity data was used during this integration.

The coordinate system used is shown in figure 3. Ideally, the two components of vorticity, ω_x and ω_y, should be measured in order to characterize the topological features of the longitudinal vortices. However, the streamwise vorticity component, ω_x, is extremely difficult to measure using the present method because of the high velocity component out of the (y, z)-plane (figure 3), at $x > 2D$. On the other hand, as shown in figure 3, it can be seen that the longitudinal vortices are inclined structures in the (x, y)-plane, so the structures should be intersected by the (x, z)-plane (defined as transverse plane). The transverse vorticity component, ω_y, will contain the footprint

of the longitudinal vortices. Efforts have therefore been focused on the transverse plane for the instantaneous velocity field measurements.

Data were taken in the centreline transverse plane ($y = 0$), approximately $2D$ from the rear of a cylinder, as shown schematically in figure 3. This region corresponds to an area of 26×21 mm^2 with a resultant resolution of the velocity vector field corresponding to a grid size of less than 0.5 mm. Such resolution is important to accurately determine the vorticity field.

The transverse vorticity component was defined as

$$\omega_y = \frac{\partial u_z}{\partial x} - \frac{\partial u_x}{\partial z}. \tag{1}$$

The vorticity at a grid point (i,j) was found numerically from the discrete velocity data using a finite difference scheme, by applying the Stokes law relating the vorticity to circulation ($\omega = \Gamma/\Delta A$):

$$\xi_y = \frac{D}{4U_0 \delta L}[((u_x^{i-1,j-1} + u_x^{i+1,j-1})/2 + u_x^{i,j-1}) - ((u_x^{i-1,j+1} + u_x^{i+1,j+1})/2 + u_x^{i,j+1})$$

$$-((u_z^{i-1,j-1} + u_z^{i-1,j+1})/2 + u_z^{i-1,j}) + ((u_z^{i+1,j-1} + u_z^{i+1,j+1})/2 + u_z^{i+1,j})] \tag{2}$$

where δL is the grid spacing and the vorticity was normalized by D, the diameter of the cylinder, and by U_0, the free-stream velocity. An uncertainty analysis of the vorticity estimates uncertainties of the order of 20% (Wu 1994).

The vorticity of the longitudinal vortices was estimated as

$$\omega = \omega_y/\sin(\alpha) \tag{3}$$

where α is the angle the longitudinal vortices make with the streamwise (x) direction. Circulation was calculated from

$$\Gamma = \int \boldsymbol{\omega} \cdot \boldsymbol{n} \mathrm{d}s = \int \omega_y \mathrm{d}x\mathrm{d}z \tag{4}$$

where s is the area of surface integration and $\boldsymbol{n}$ is a unit vector normal to the surface. From this it can be seen that the circulation calculated in the transverse plane of measurement represents the total circulation of the inclined longitudinal vortices. The circulation of a longitudinal vortex has been estimated by integrating vorticity over the area in which ξ_y is greater than 10% of ξ_{ymax}, the peak vorticity of the vortex. To obtain a general description of the statistics of the longitudinal vortices, images were sampled in two ways. In one, samples were taken randomly in time at a given spatial location. In the other, samples were phase-locked to the Kármán vortex shedding cycle. This was achieved by triggering the acquisition of PIV images with the signal from a hot-film probe placed in the wake of the cylinder.

3. Results

3.1. *Character of the vortices*

Results for two particular images, acquired at a Reynolds number of 525 and at different random points in the phase of the Kármán vortex shedding cycle, are presented in figure 4 and figure 5; there is clearly a similarity between the two cases. While the vortices appear remarkably regular in streamwise location and spanwise spacing, there is also a variability due to the distortion of the vortex street. In figure 4(a) (refer to figure 3 for the plane of measurement) the velocity field in the (x, z)-plane is shown. Though smaller than the streamwise component, the spanwise
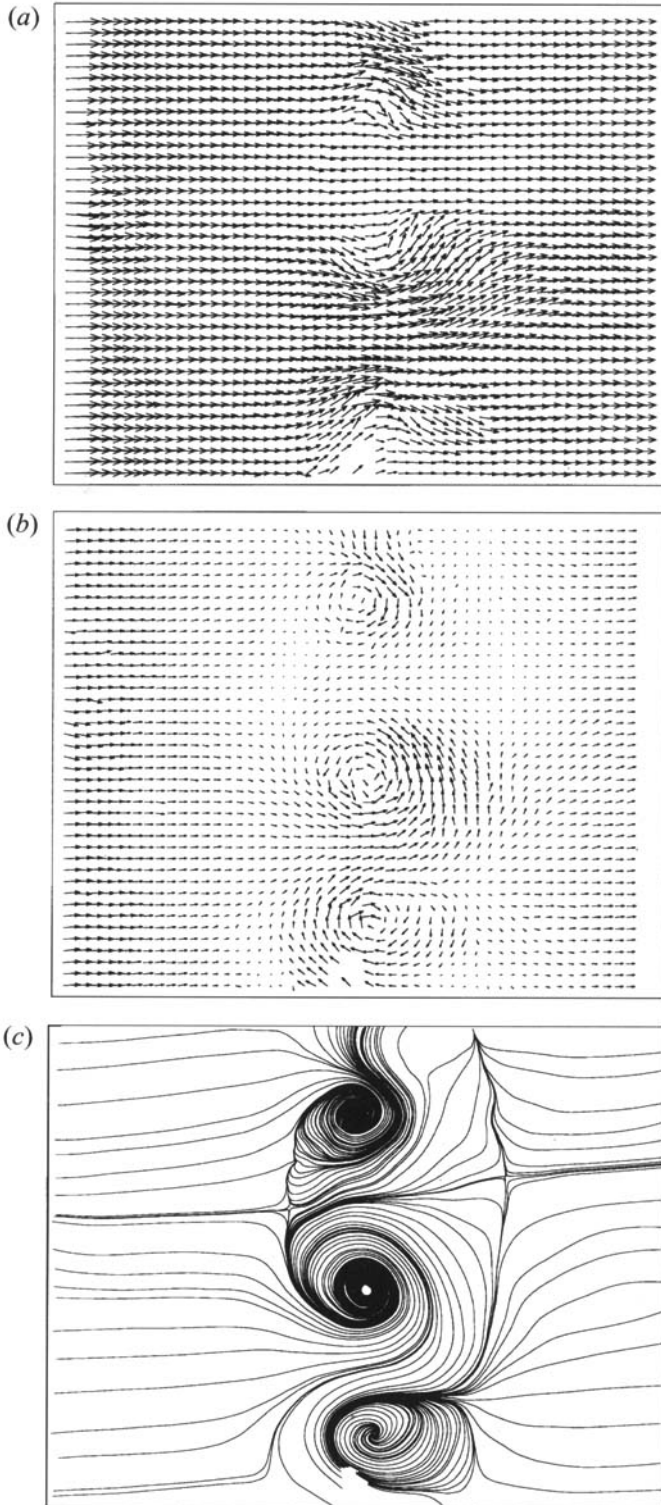
(a)

(b)

(c)

FIGURE 4. Measured velocity field in the transverse plane (x, z-plane) taken at a single instant: (a) seen in a stationary frame of reference; (b) seen in a frame of reference moving at $60\%U_0$; (c) sectional streamlines in the moving frame of reference at 60% of U_0.
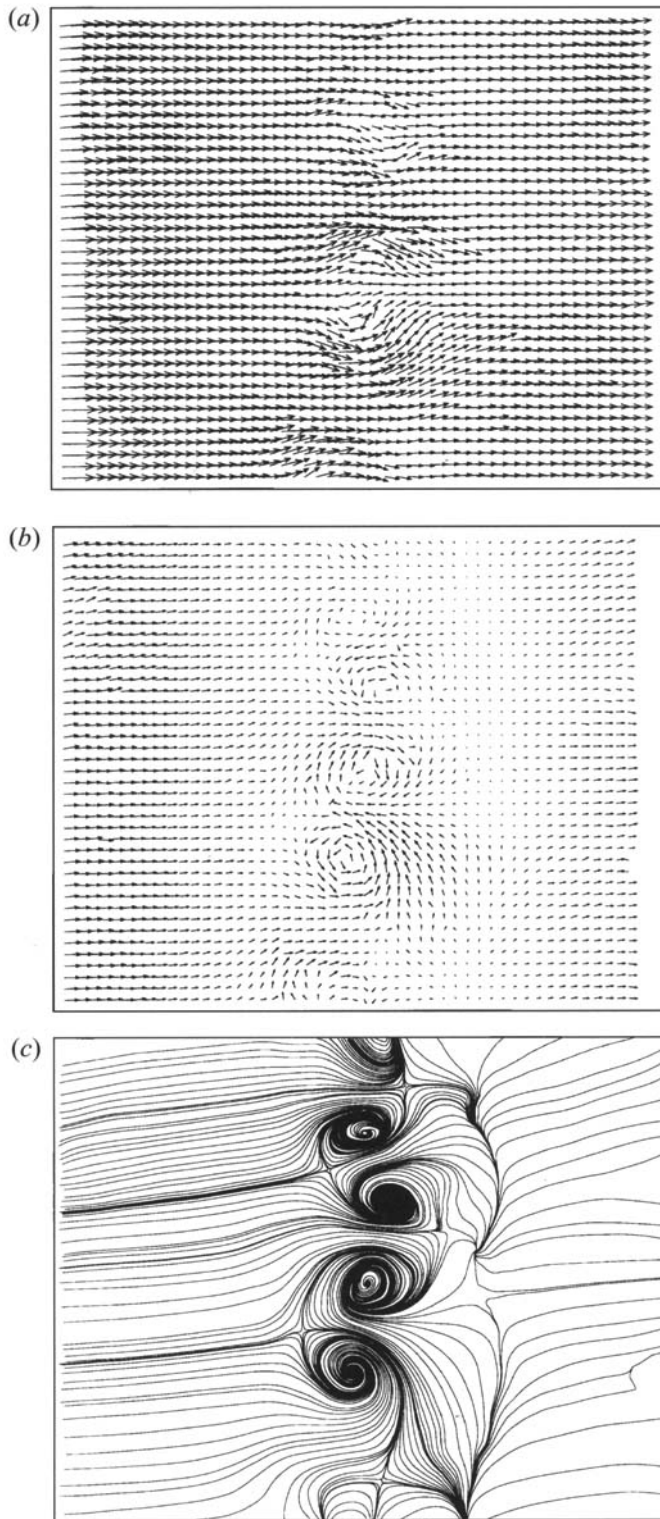
(a)

(b)

(c)

FIGURE 5. Measured velocity field in the same plane and for the same experimental conditions as in figure 4. Counter-rotating vortices of a similar nature to those in figure 4 can be seen in (a), (b) and (c), which are as described in the caption to figure 4. Because the fields in the two figures are instantaneous ones, however, there are noticeable differences between the two sets of vortices.
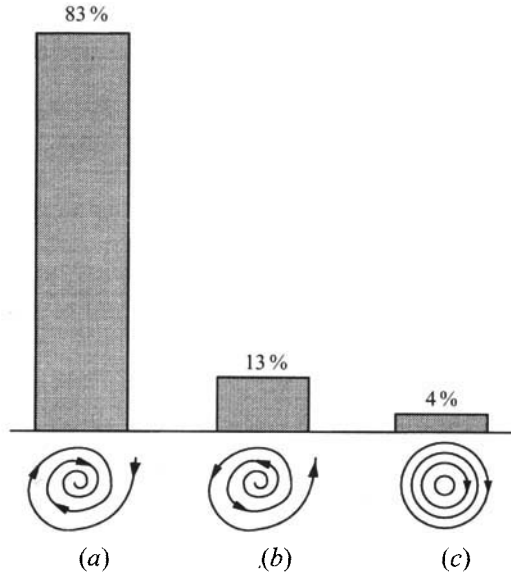
FIGURE 6. Survey of the topology of the foci of the longitudinal vortices, using sectional streamlines: (a) spiralling in, stable focus; (b) spiralling out, unstable focus; (c) limit cycle. The measured distributions of the different topological features are given in the histograms above the schematics.

component of velocity, u_z, is seen to be significant. When the eddy convection velocity is removed, as in figure 4(b), the footprint of the longitudinal vortices becomes clearly evident. An averaged value of 60% of the free-stream velocity was taken as the convection velocity. This is consistent with other studies but it is recognized that the vortices convect with a range of speeds between 50% and 70% of the free-stream, residing as they do (to be discussed later) in the low-speed region between Kármán vortices. As expected from the mushroom-type structures seen in the flow visualizations, the vortices appear as counter-rotating pairs, with each vortex rotating in the direction opposite to its neighbours.

Corresponding instantaneous sectional streamlines are shown in figure 4(c). (It should be noted that the streamlines presented are *not at constant intervals of the stream function.*) These are presented in the same moving frame of reference as the velocity fields in figure 4(b). In general the streamlines indicate that there are regions of two-dimensional vortex shedding, evident by the existence of the streamlines parallel to the streamwise direction. Embedded within these, however, are regions in which the flow streamlines distort as they spiral around foci, indicative of the existence of counter-rotating longitudinal vortices. These foci provide information on the flow structure, as discussed later. Similar flow patterns are revealed in figures 5(a), 5(b) and 5(c). Note, however, the change in instantaneous spanwise spacing of the longitudinal vortices.

Using the description of flow patterns based on the critical point terminology of Perry & Fairlie (1974), there are three ways in which streamlines can behave close to a focus. When the streamlines spiral in, as shown in figure 6(a), the vortex represented by the streamlines experiences axial expansive strain. Such a vortex is stable and the vorticity is amplified owing to the stretching. However, when the streamlines spiral out, as shown in figure 6(b), the vortex represented by the focus is subjected to axial compressive strain. This tends to buckle the vortex filament, as shown by Rogers &
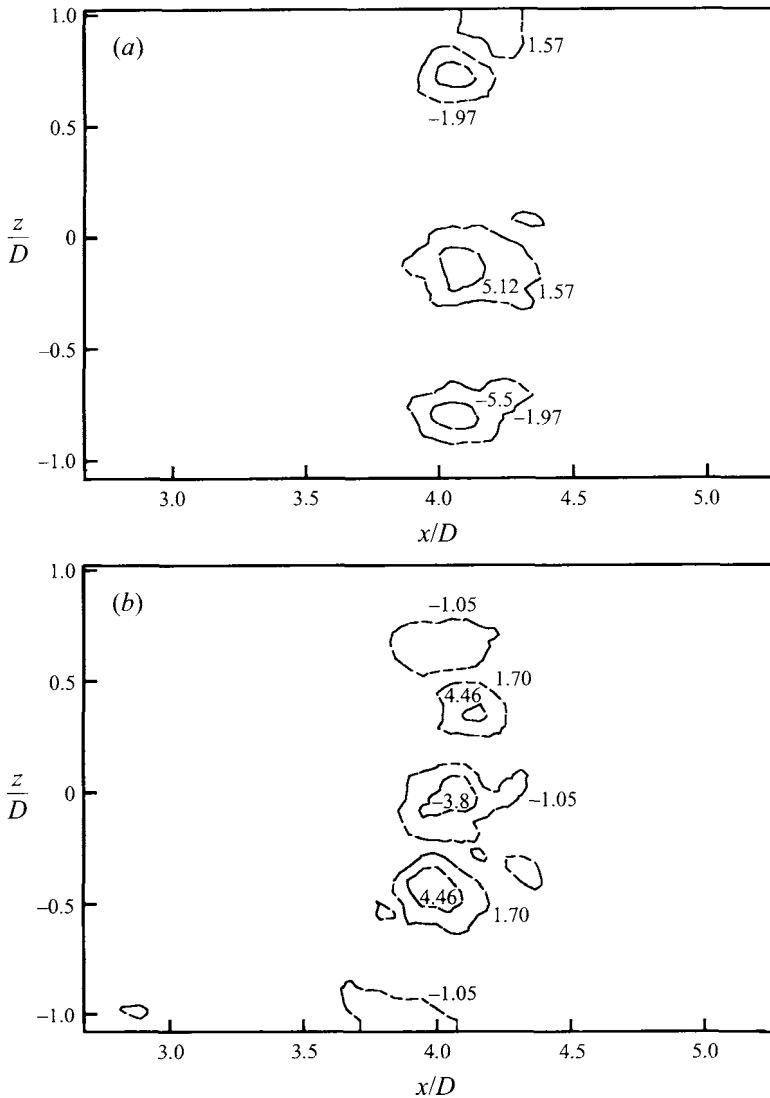
FIGURE 7. Normalized y-component instantaneous vorticity contours in the centreline plane at $Re = 525$. Vorticity field: (a) corresponds to the measured velocity field of figure 4 and (b) corresponds to the field of figure 5.

Moin (1987) using data bases produced by direct numerical simulations. Such foci are unstable. The third possibility is when the streamlines form limit cycles, as shown in figure 6(c), such foci being neutrally stable.

To characterize the topological behaviour of the flow near the foci formed by the longitudinal vortices, 50 frames of velocity distributions, such as those shown in figures 4 and 5, were classified into the three categories of foci. The results are shown in figure 6. In 83% of cases the streamlines spiral in towards the critical point, 13% spiral out, and 4% approach a limit cycle. We conclude from this that the cores of most of the longitudinal vortices intersecting the centreline transverse plane ($y = 0$) are being stretched normal to the plane of measurement.

Vorticity contours of the flow fields are presented in figure 7, corresponding to the
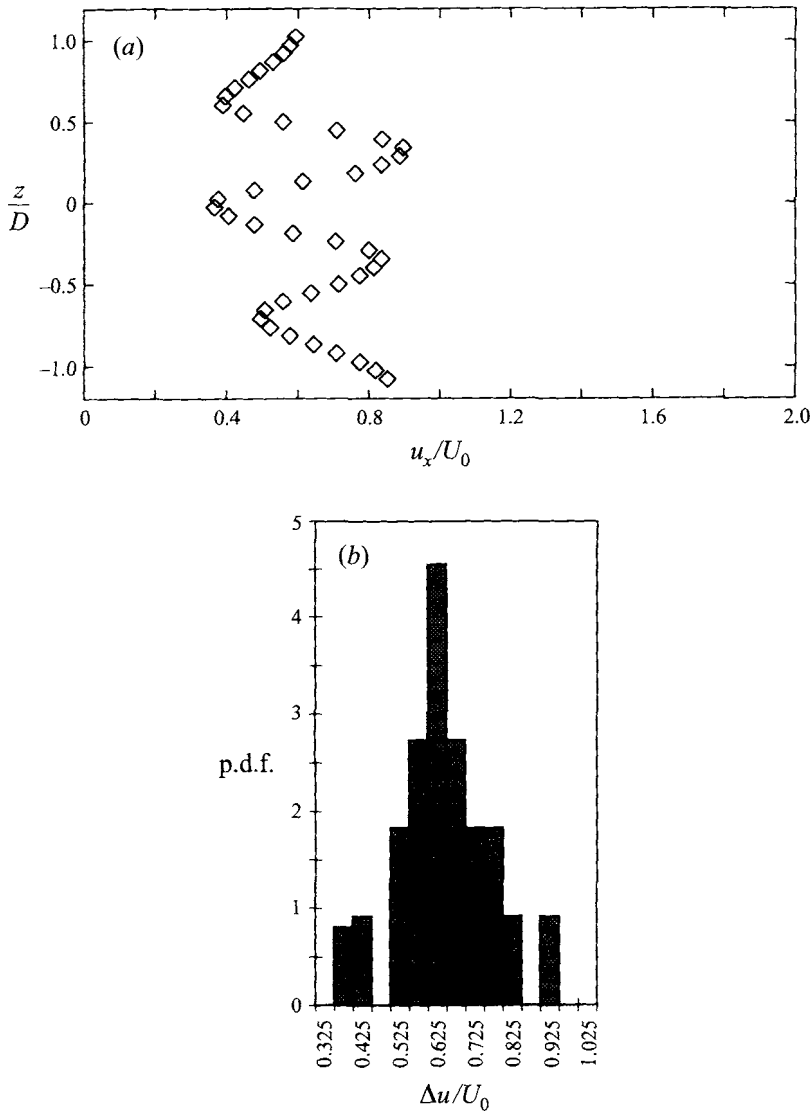
FIGURE 8. The u_x spanwise distributions through vortex centres: (a) a typical spanwise profile; (b) probability density function of modulation amplitude.

two data frames in figure 4 and figure 5. Vortices appear in pairs or in bands of matched vortices with similar vorticity levels but of alternating sign. The bands of vortices remain parallel to the cylinder axis at the measurement plane. This is due to the control exerted by the forcing from the large-scale Kármán vortices. However, while regularly spaced in the spanwise direction, the vortices appear not to be fixed at spanwise locations. When observed during experiments, the longitudinal vortices appeared to 'wander' along the span of the cylinder. Previous attempts to lock the vortices to an applied spanwise perturbation, as described by Wu *et al.* (1994a), were unsuccessful.

To show the spanwise velocity variation caused by the existence of the longitudinal vortices, a typical instantaneous velocity profile through the centres of longitudinal vortices is shown in figure 8(a). The probability density function of the modulation

amplitude Δu, which is defined as the difference between the maximum and minimum velocity, was also calculated and is shown in figure 8(*b*). It is estimated that the amplitude of velocity spanwise modulation is approximately $0.63U_0$. As a comparison, the streamwise variation of spanwise-averaged velocity profiles, which are associated with Kármán vortices, are plotted in figure 9 and will be discussed later.

Velocity spanwise profiles are rarely measured in wakes, partly because of the difficulty of capturing three-dimensional features using conventional single-point probes. However, there has been some success in using single sensors to measure the time-mean spanwise velocity profile in mixing layers. Huang & Ho (1990) studied the small-scale transition process of a mixing layer using an X-wire probe. They measured the spanwise distribution of the time-mean streamwise velocity profile. The profiles were found to contain clear wavy patterns, which as they pointed out were due to the formation of streamwise vortices (longitudinal vortices). The amplitude of the wavy pattern varies from $0.1\bar{U}$ to $0.2\bar{U}$ (where $\bar{U}$ is the mean velocity of the mixing layer), depending on streamwise distance. It appears therefore that the velocity amplitude of the spanwise modulation is larger in wakes than in mixing layers.

3.2. *Relationship to the Kármán vortices*

As a first step toward understanding the complex wake flows, it is important that the relationship between the various vortical structures found in the wakes of cylinders be determined. Also important, from the perspective of macroscopic quantities such as drag and heat transfer, are the relative strengths of the vorticity fields resulting from each class of vortex. In this section the phase relationship that the longitudinal vortices bear to the Kármán vortices will be examined, as will their orientation to each other in space. The levels of vorticity and circulation in the two sets of vortices will also be quantified. While the longitudinal vortices are not fixed in space in the spanwise direction, the results of previous flow visualizations conducted by Wu *et al.* (1994*a*) suggested that they have the same frequency as the Kármán vortices. It is therefore reasonable to conclude that there is a spatial relationship between the two sets of vortices in the streamwise direction, despite the randomness in the spanwise direction. The streamwise velocity component averaged across the span can be used to characterize the streamwise evolution of the vortex street:

$$\bar{u}_x(x, 0, T) = \frac{1}{L} \int_0^L u_x(x, 0, z, T)\mathrm{d}z \tag{5}$$

where L ($\approx 2.2D$) is the spanwise length of the measurement plane, T denotes time and $y = 0$. Typical x-variations of $\bar{u}_x(x, 0, T)$ are shown in figure 9. The streamwise variation in $\bar{u}_x(x, 0, T)$ can be used to detect the formation of the vortex street. The phases of the spanwise vortices shed from the cylinder are not fixed, since each measurement frame was sampled randomly. The x-coordinate at which $\bar{u}_x(x, 0, T)$ is a minimum is used to characterize the streamwise distance of the shedding Kármán vortices:

$$x_{KM} = x|_{\bar{u}_x(x,0,T)=min[\bar{u}_x]}. \tag{6}$$

The parameter x_{KM} can also be considered as a phase tag for the shed vortex. It is the streamwise location (in the $y = 0$ plane) of the tagged phase of the Kármán vortex street. The streamwise position of longitudinal vortices is defined as the point at which the centroid of an identified longitudinal vortex pair is detected (where ξ_y peaks); this is denoted as x_{LV}. A correlation between x_{KM} and x_{LV} is plotted in figure 10. On the graph, the line drawn with unit gradient corresponds to the case where
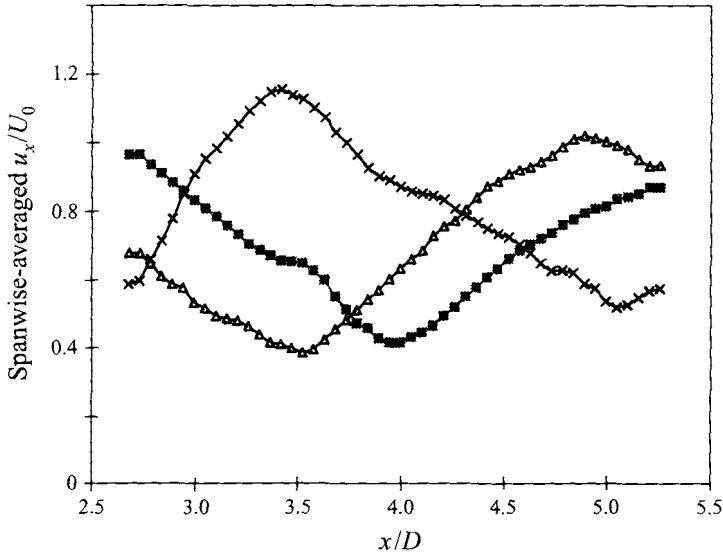
FIGURE 9. Streamwise variation of $\bar{u}_x$ induced by the background Kármán vortex street. Shown are three samples, arbitrarily selected from the data set but having the Kármán vortices at different streamwise locations.
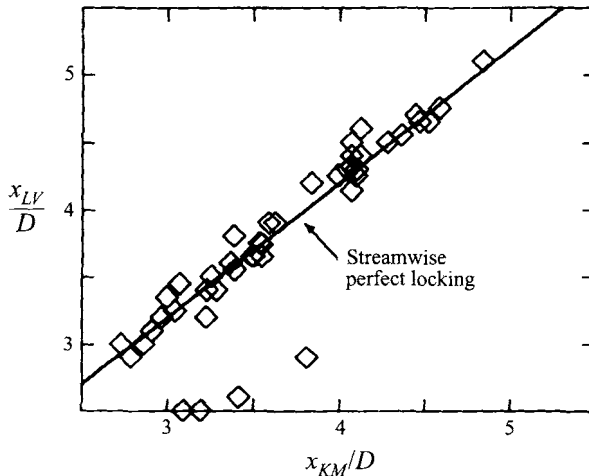

FIGURE 10. Phase correlation between the Kármán vortices and embedded longitudinal vortices. x_{KM} is the streamwise location of a tagged point in the Kármán vortices while x_{LV} is the location of the embedded longitudinal vortices.

the longitudinal vortices are locked perfectly to Kármán vortices in the streamwise direction. The data are seen to be distributed close to the ideal correlation line, indicating that longitudinal vortices are indeed locked spatially to Kármán vortices in the x-direction, even though they may be randomly located in the spanwise direction. Therefore, the longitudinal vortices must have streamwise periodicity, since Kármán vortices are spatially periodic in the x-direction. For a stationary observer, therefore, the longitudinal vortices will usually have the same frequency as the Kármán vortices. This result confirms that the two sets of vortices are spatially related. It can also be concluded from the graph that the section of the longitudinal vortices in the laser sheet plane (i.e. centreline plane of the cylinder) are located slightly downstream of
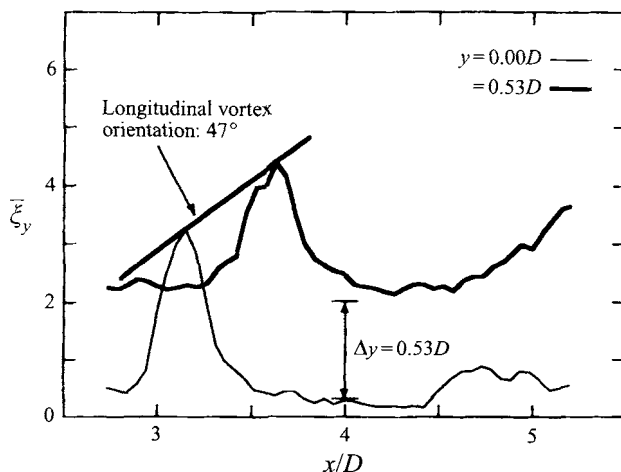
FIGURE 11. Distributions of transverse vorticity, $\bar{\xi}_y(x)$, in the streamwise direction at two
y-positions across the wake, $Re = 544$.

the point where the minimum convective velocity occurs, i.e.

$$x_{LV} \approx x_{KM} + 0.2D. \tag{7}$$

By examining all the data samples it was found that $\bar{u}_x$ varies from $0.5U_0$ to $0.7U_0$ at
$x = x_{KM} + 0.2D$. This was the basis on which an averaged value $0.60U_0$ was used for
the moving frame of reference in the previous presentation.

In a different set of experiments aimed at determining the inclination angle of the
longitudinal vortices, a hot-film probe was placed in the wake to detect the phase of
Kármán vortex shedding from the cylinder. Images were acquired when the hot-film
signal crossed zero with positive slope. Images from the two planes, one at $y = 0$
(centre-line) and the other at $y = 0.53D$ (close to the wake edge) were obtained to
calculate the spanwise-averaged vorticity at an instant T:

$$\bar{\xi}_y(x, y, T) = \frac{1}{L} \int_0^L |\xi_y(x, y, z, T)| \mathrm{d}z \tag{8}$$

where $y = 0$ or $y = 0.53D$. The result is shown in figure 11; the curve at $y = 0.53D$ is
offset to highlight the fact that its image plane was located above the wake centreline.
The location of the peak vorticity at $y = 0.53D$ is clearly shifted by $\delta x \approx 0.5D$ in the
streamwise direction. This gives an inclination angle of $47 \pm 9°$, where the variance
was due to the phase jitter during the triggered sampling.

Several attempts have been made to measure the inclination angle of the longitu-
dinal vortices in the wake of a bluff body. Hayakawa & Hussain (1989) suggested
that they were inclined at an angle of $60°$ to the x-axis, while Wu *et al.* (1994*a*), using
flow visualization, and Zhou & Antonia (1992), using hot-wire anemometry, found
the inclination angle to be approximately $55°$. The result obtained from this study
suggests that the inclination angle is approximately $50°$ in the near-wake region close
to the centreline of the cylinder at low Reynolds numbers. Discrepancies between the
results from different studies are perhaps expected in the light of the unsteady nature
of the flows and the differences in the measurement conditions (such as Reynolds
number, cylinder aspect ratio). Nevertheless, these data support the hypothesis of
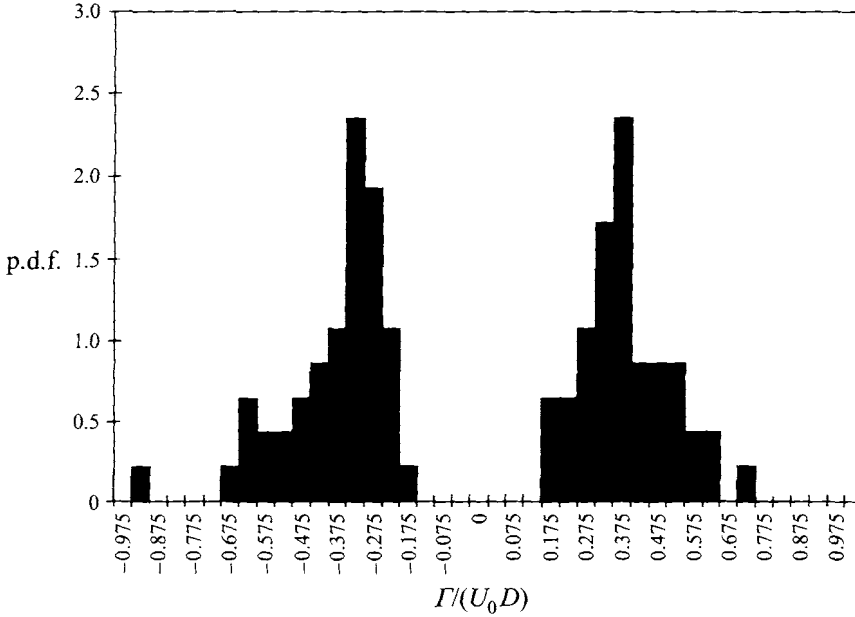Wu *et al.* (1994*a*), derived from the vortex dynamics model, that a distorted vortex

FIGURE 12. Probability density function of the circulation of the longitudinal vortices at $Re = 525$.

$\Gamma_+/(U_0 D)$	0.38 ± 0.24
$\Gamma_-/(U_0 D)$	-0.39 ± 0.30
$|\Gamma_{KM}|/(U_0 D)$	$\approx 3.5 \pm 0.53$

TABLE 1. Averaged circulation of longitudinal vortices and circulation of the Kármán vortices; the uncertainties are calculated at a confidence level of 95%.

filament eventually reorientates to align with the positive principle axis of the strain field near the saddle point of the spanwise vortices.

Wu *et al.* (1994*b*) used the same PIV technique to measure the velocity field in the (x, z)-plane of the wake. From these measurements the levels of vorticity in the spanwise direction, resulting from the Kármán vortices, was found. For Reynolds numbers between 150 and 660, the Kármán vortices had a maximum spanwise vorticity of approximately $\xi_{zmax} = 4 \sim 5$. At a Reynolds number of 525, the longitudinal vortices were found to have (y-component) vorticity levels of $\xi_y \approx 7.3$ measured in the transverse plane. Assuming the longitudinal vortices are inclined at 50° to the streamwise direction, the peak vorticity in the longitudinal vortices, i.e. the maximum vorticity aligned with their axis, is estimated to be $\xi \approx 9.5$ (using (3)). Thus, the vorticity of the longitudinal vortices is approximately twice that of the Kármán vortices, on which they are carried.

Figure 12 shows the probability density function of circulation. The average circulations were calculated together with the variance caused by velocity fluctuations and are presented in table 1, where the subscripts $_+$ and $_-$ denote the positive and negative vorticity respectively. The circulation of the spanwise vortices (Kármán vortices, denoted by the subscript KM) is included for comparison. It can be seen that the circulation of the longitudinal vortices is significantly smaller than that of the

Kármán vortices:

$$\frac{\Gamma}{\Gamma_{KM}} \approx 0.11 \qquad (9)$$

where Γ stands for the circulation of the longitudinal vortices (the sign having been dropped).

Few published results have been found to date on the circulation of longitudinal vortices in wakes. On the other hand, the circulation of longitudinal vortices in mixing layers has been presented by Jimenez, Cogollos & Bernal (1985). That study investigated the three-dimensional topology of the streamwise vortices in a plane mixing layer. It was found, using a method of estimation based on visualized mushroom-type patterns, that the ratio between the circulation of the streamwise vortices and the spanwise vortices was 0.6. This value is considerably larger than that found in the wake, as presented above. Thus, it would appear that there is a fundamental difference between the longitudinal vortices found in wakes and mixing layers.

3.3. *Effect of Reynolds number*

In a study of cylinder wakes, Williamson (1988) found that there are two stages in the transition to three-dimensionality in the wake. He found what he terms Mode 'A' at Reynolds numbers greater than 170, this mode being characterized by a spanwise wavelength of approximately $3D$. At $Re = 230$–260 he found a second transition to a shorter wavelength, $1D$, Mode 'B'. Evidence in support of this two-stage transition has now been provided in the numerical work of Thompson *et al.* (1994). Mansy *et al.* (1994) also found experimental evidence of Mode B. Figure 13(a–c) shows the typical instantaneous streamlines with the eddy convection velocity removed for Reynolds numbers of 137, 204 and 394. This spans the transition regime discussed above. At $Re = 137$, the Kármán vortices are fully formed but there is no sign of the longitudinal vortices; the vortex shedding appears to be two-dimensional with parallel streamlines. At $Re = 204$, the velocity field shows evidence of a velocity component in the spanwise direction. While this Reynolds number places the flow in Williamson's Mode A, there is not enough regularity in the vortex structures to reliably measure the spanwise wavelength. It should be noted that the aspect ratios of the current set of experiments may be too low to get Mode A shedding. At $Re = 395$, the longitudinal vortices are now regular, and well-formed, and it would appear that at this Reynolds number the transition from a two-dimensional to a three-dimensional wake is complete.

To examine this transition quantitatively, the effect of Reynolds number on the circulation of the longitudinal vortices was measured. PIV measurements were made in the same transverse plane as previously for Reynolds numbers ranging from 140 to 550. The results are shown in figure 14(a), where the absolute values of the normalized circulations are plotted against Reynolds number. The data point at $Re = 525$ is an average of 50 samples, and the remaining points are, typically, averages of 5 samples. It is seen that there is a transition in the range of $Re = 150$–300, where $|\Gamma|/(U_0 D)$ increases from approximately zero at $Re = 150$ to 0.4 at $Re = 300$. For $Re > 300$, the circulation remains approximately constant, at least up to $Re = 550$. The process of the transition corresponds to the onset of the longitudinal vortices.

Figure 14(b) shows the maximum transverse vorticity ξ_{ymax} variation with Reynolds number, where ξ_{ymax} is defined as

$$\xi_{ymax} = \max[\xi_y(x,z)]. \qquad (10)$$

At Reynolds numbers below 200, ξ_{ymax} is low and there is no sign of organized

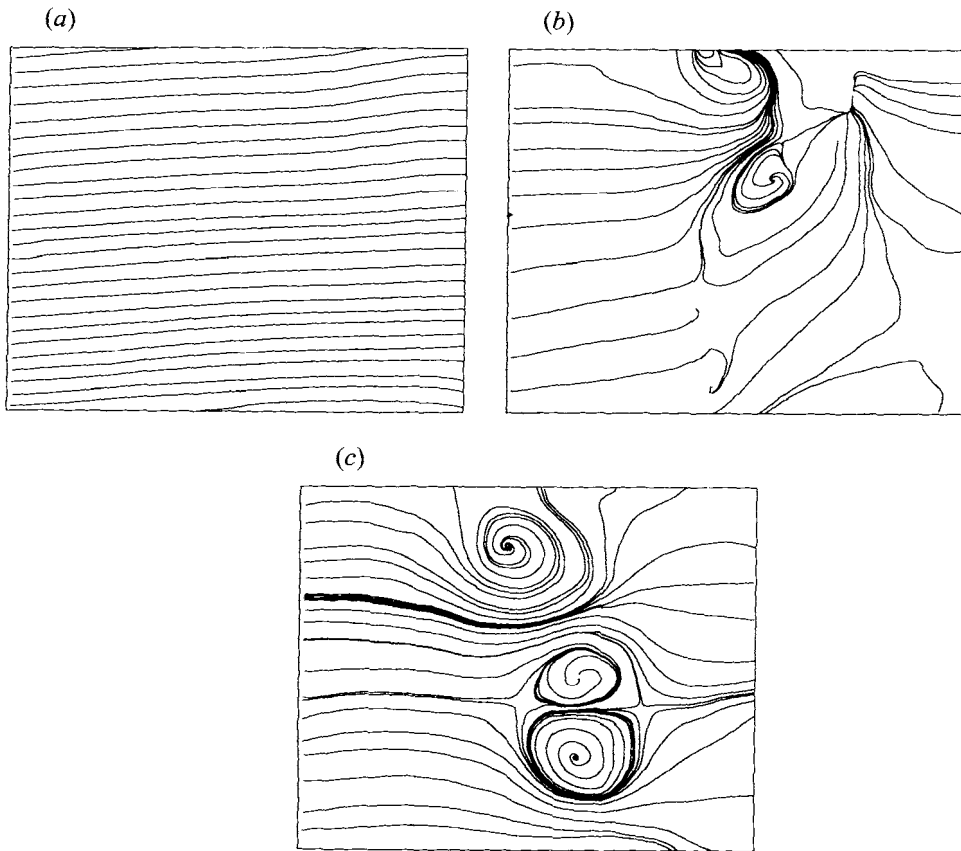(a)   (b)

(c)

FIGURE 13. Flow field variation with Reynolds number: (a) $Re = 137$, (b) $Re = 204$, (c) $Re = 394$. Sectional streamlines are shown in the frame of reference moving at 60% of U_0.

vorticity concentration. However, there is a marked increase in ξ_{ymax} between Reynolds numbers of 200 and 250. As seen previously, this vorticity is concentrated in the vortex pairs which are the footprints of the longitudinal vortices. The increase saturates at approximately $Re = 250$, where ξ_{ymax} reaches $6 \sim 8$. This transition range coincides with the Reynolds number range at which Williamson (1988) found the transition from Mode A to B. Based on these results, the previous flow visualizations of Williamson (1988) and Wu *et al.* (1994a), the measurements of Mansy *et al.* (1994), and the numerical study of Thompson *et al.* (1994), a more complete picture of the transition process now emerges. As the Reynolds number increases to $150 \sim 170$, longitudinal vortices start to emerge from an initially two-dimensional laminar vortex street. Initially, the vortices are weak with low vorticity, i.e. $\xi_{ymax} < 2.0$, and are irregular and intermittent. As the Reynolds number increases to approximately 250 the vortices become fully developed and the vorticity increases to $\xi_{ymax} \approx 6 \sim 8$. Further increases in Re do not change the normalized vorticity ξ_{ymax}, implying a linear correlation: $\omega_y \propto U_0/D$, since the vorticity has been normalized as $\xi_y = \omega_y/(U_0/D)$.

It is also noted that this vorticity transitional region corresponds to the 'transition range' of Roshko (1955) ($Re = 150$–300). In this range Roshko found that there were irregular bursts of velocity in the wake, the bursts being more violent as the Reynolds number increased. Similar results were reported by Bloor (1964), based on hot-wire data taken at Reynolds numbers from 200 to 400.
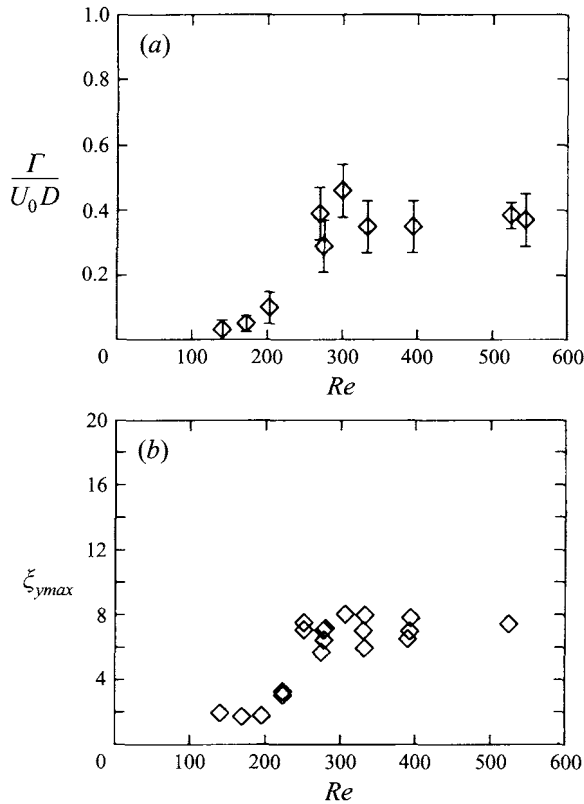
FIGURE 14. Variation of the circulation and vorticity of the longitudinal vortices with *Re*:
(*a*) ensemble-averaged circulation, error bars denote uncertainty; (*b*) vorticity.

3.4. *The evolution of longitudinal vortices in a wake*

In an attempt to better understand the evolution of the longitudinal vortices in a bluff-body wake, Wu *et al.* (1994*a*, *c*) proposed that they could be modelled using a simple vortex filament method. This is shown schematically in figure 15, in a frame of reference moving with the vortices. This simplified model has two fundamental elements: (i) a perturbed vorticity tube; and (ii) a stretching region near the saddle point (denoted by S) formed by the primary, spanwise vortices. Initially, a fluid tube containing vorticity (vorticity tube) is located at position 1, normal to the plane of the page. Above a critical Reynolds number, any non-uniformity in the flow disturbs the vorticity tube causing it to develop a kink. As time elapses, the perturbed vorticity tube, moving at the local convection velocity, arrives at position 2 and the amplitude of the kink grows owing to self-induction of the tube, in accordance with the Biot-Savart law. As the distorted tube approaches the strain field near the saddle point, the spanwise vortices are stretched, resulting in higher vorticity levels. The process is most pronounced when the vorticity tube is being 'pulled apart' in *opposite directions* along the diverging separatrix. This is shown in figure 15 where the flows in regions A and B are moving in opposite directions in the moving frame of reference. Finally, counter-rotating longitudinal vortices, inclined to the streamwise direction, are formed at position 3.

According to the present measurements, the circulation of a longitudinal vortex is found to be only 11% of the circulation of a Kármán vortex. This suggests that only
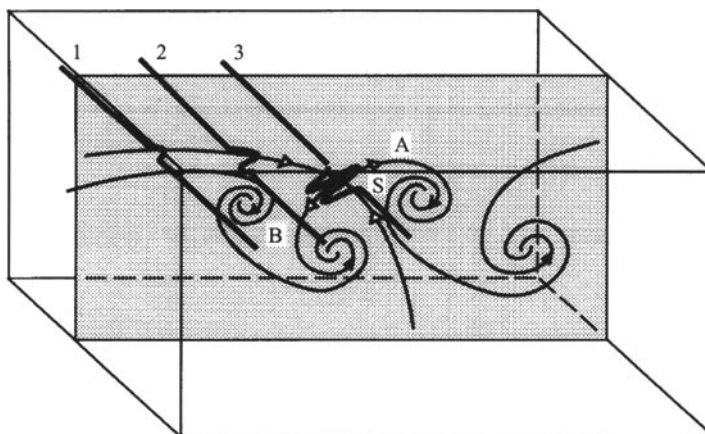
FIGURE 15. Schematic showing the basis of the vortex filament model. A vortex filament with a minor perturbation at 1 develops a kink; 2 growth of the kink due to self-induction of the filament; 3 significant stretching at the saddle point S.
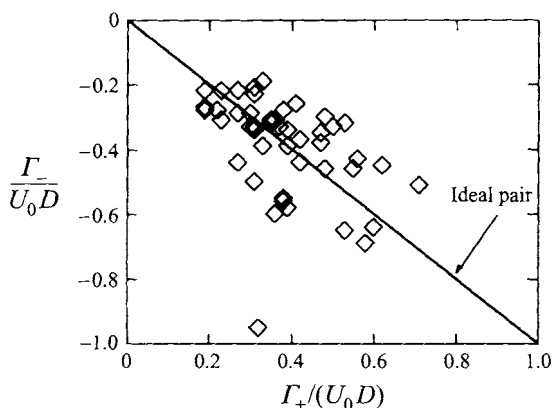

FIGURE 16. Circulation correlation: the circulations are taken from the two vortices constituting vortex pairs.

part of a spanwise vortex is involved in the process of distortion and stretching that forms the counter-rotating longitudinal vortices. Since the circulation is independent of time, by Kelvin's law, it is clear that the circulation of the developed longitudinal vortices should be smaller than that of the spanwise vortices.

Based on this model, a number of hypotheses, which could be tested experimentally, can be proposed. The primary one tested here is that if such a model were to be valid, the pairs of counter-rotating vortices, found in the measurement plane, should have circulations that are of equal and opposite sign. This condition arises from the fact that they are part of the same material vortex tube and circulation is invariant in time and invariant along a vortex loop, no matter how much it is distorted. Since the present technique can be used to measure the instantaneous velocity field of a vortex pair, it is possible to study the correlation of circulation between the two vortices of vortex pairs. The circulations of both positive and negative vortices in a vortex pair are plotted against each other in figure 16. A vortex pair is said to be ideally matched if its positive and negative circulations are equal. This would be indicated by a line on the graph of slope -1. The data points, although showing a degree of scatter, indicate

a clear trend of linear correlation. Thus, an increase in the circulation of one vortex of a counter-rotating vortex pair corresponds to an increase (in absolute value) in the circulation of the other vortex of the same pair. The result is consistent with the hypothesis and indicates that the vortices, appearing as mushroom-type structures in the flow visualizations, are indeed part of a vortex loop.

4. Conclusions

Results have been presented which characterize the longitudinal vortices found between the Kármán vortices in the wake of circular cylinders at low Reynolds numbers. In particular, they are shown to have levels of vorticity that can be double that of the Kármán vortices while the levels of circulation are typically an order of magnitude less ($\approx 11\%$). The high levels of vorticity are consistent with a vortex dynamics model, i.e. the evolution of the longitudinal vortices from a distortion of the vorticity in the separating shear layers. From a detailed study of the footprint of the longitudinal vortex pairs, it is shown that the pairs' circulations are matched in magnitude but of opposite sign – again consistent with the model. The longitudinal vortices are phase-locked to the Kármán vortices and appear to be aligned with their positive principal axis of the strain. While no visual evidence is presented of the two modes in transition to three-dimensionality, there is evidence that for Reynolds numbers between 200 and 250 there is a large increase in vorticity and circulation of the longitudinal vortices. Finally, the results show that the study of low Reynolds number wakes has significance for the production of turbulence in wakes by illustrating the important role of vortex stretching in such wakes.

REFERENCES

ADRIAN, R. J. 1991 Particle-imaging techniques for experimental fluid mechanics. *Ann. Rev. Fluid Mech.* **23**, 261–304.

BAYS-MUCHMORE, B. & AHMED, A. 1993 On streamwise vortices in turbulent wakes of cylinders. *Phys Fluids* A **5**, 387–392.

BERNAL, L. P. & ROSHKO, A. 1986 Streamwise vortex structure in plane mixing layers. *J. Fluid Mech.* **170**, 499–525.

BLOOR, M. S. 1964 The transition to turbulence in the wake of a circular cylinder. *J. Fluid Mech.* **19**, 290–304.

GERRARD, J. H. 1978 The wakes of cylindrical bluff bodies at low Reynolds number. *Trans. R Phil. Soc. Lond.* **288**, 351–382.

GONZE, M. A. 1993, PhD thesis, National Polytechnic Institute, Grenoble. (Reproduced in Green, S. I. 1995 *Fluid Vortices*, p. 52. Kluwer).

GRANT, M. L. 1958 The large eddies of turbulent motion. *J. Fluid Mech.* **4**, 149–190.

HAMA, F. R. 1957 Three-dimensional vortex pattern. *J. Aero. Sci.* 156–158.

HAYAKAWA, M. & HUSSAIN, F. 1989 Three-dimensionality of organized structures in a plane turbulent wake. *J. Fluid Mech.* **206**, 375–404.

HUANG, L.-S. & HO, C.-M. 1990 Small-scale transition in a plane mixing layer. *J. Fluid Mech.* **210**, 475–500.

JIMENEZ, J., COGOLLOS, M. & BERNAL, L. P. 1985 A perspective view of the plane mixing layer. *J. Fluid Mech.* **152**, 125–143.

KARNIADAKIS, G. E. & TRIANTAFYLLOU, G. S. 1992 Three-dimensional dynamics and transition to turbulence in the wake of bluff objects. *J. Fluid Mech.* **238**, 1–30.

LIN, J.-C., VOROBIEFF, P. & ROCKWELL, D. 1995, Three-dimensional patterns of streamwise vorticity in the turbulent near-wake of a cylinder. *J. Fluids Struct.* **9**, 231–234.

MANSY, H., YANG, P.-M. & WILLIAMS, D. R. 1994 Quantitative measurements of three-dimensional structures in the wake of a circular cylinder. *J. Fluid Mech.* **270**, 277–296.

MEIBURG, E. & LASHERAS, J. C. 1988 Experimental and numerical investigation of the three-dimensional transition in plane wakes. *J. Fluid Mech.* **190**, 1–37.

PERRY, A. E. & FAIRLIE, B. 1974 Critical points in flow patterns. *Adv. Geophys.* **B14**, 299–315.

PERRY, A. E. & STEINER, T. R. 1987 Large-scale vortex structures in turbulent wakes behind bluff bodies. Part 1. Vortex formation process. *J. Fluid Mech.* **174**, 233–270.

ROGERS, M. & MOIN, P. 1987 The structure of the vorticity field in homogeneous turbulent flows. *J. Fluid Mech.* **176**, 33–66.

ROSHKO, A. 1955 On the development of turbulent wakes from vortex streets. *NACA Rep.* 1191, pp. 801–825.

THOMPSON, M., HOURIGAN, K. & SHERIDAN, J. 1994 Three-dimensional instabilities in the wake of a circular cylinder. *Exp. Thermal Fluid Sci.* (in press).

WEI, T. & SMITH, C. R. 1986 Secondary vortices in the wake of circular cylinders. *J. Fluid Mech.* **169**, 513–533.

WELSH, M. C., SORIA, J., SHERIDAN, J., WU, J., HOURIGAN, K. & HAMILTON, N. 1992 Three-dimensional flows in the wake of a circular cylinder. *Visualization Soc. Japan* **9**, 17–18.

WILLIAMSON, C. H. K. 1988 The existence of two stages in the transition to three-dimensionality of a cylinder wake. *Phys Fluids* **31**, 3165–3168.

WILLIAMSON, C. H. K. 1989 Oblique and parallel modes of vortex shedding in the wake of a circular cylinder at low Reynolds number. *J. Fluid Mech.* **206**, 579–627.

WU, J. 1994 Three-dimensional vortical structures in the wake of a bluff body. PhD thesis, Monash University, Australia.

WU, J., SHERIDAN, J., SORIA, J. & WELSH, M. C. 1994*a* An experimental investigation of streamwise vortices in the wake of a bluff body. *J. Fluids Struct.* **8**, 621–635.

WU, J., SHERIDAN, J., SORIA, J. & WELSH, M. C. 1994*b* An investigation of unsteady flow behind a circular cylinder using a digital PIV method. *Laser Anemometry, Advances and Applications,* ASME FED-Vol. 184, pp. 167–172.

WU, J., SHERIDAN, J. & WELSH, M. C. 1994*c* Vortex filament simulation of the longitudinal vortices found in the wake of a bluff body. *Boundary Layer and Free Shear Flows.* ASME FED-Vol. 184, pp. 187–194.

WU, J., SHERIDAN, J., WELSH, M. C., HOURIGAN, K. & THOMPSON, M. 1994*d* Longitudinal vortex structures in a cylinder wake. *Phys Fluids* **6**, 2883–2885.

ZHOU, Y. & ANTONIA, R. 1992 A study of flow properties near critical points. *Eddy Structure Identification in Free Turbulent Shear Flows, IUTAM Symp., Poitiers,* France, pp. IX.2.1–2.6.